Measurement 224 (2024) 113919

Contents lists available at ScienceDirect

Measurement

journal homepage: www.elsevier.com/locate/measurement

Comparing Mobile and Aerial Laser Scanner point cloud data sets for automating the detection and delimitation procedure of safety-critical near-road slopes

Antón Núñez-Seoane *, Joaquín Martínez-Sánchez, Erik Rúa, Pedro Arias

CINTECX, Universidade de Vigo. Applied Geotechnologies Group, Vigo, 36310, Spain

ARTICLE INFO

Keywords:
Automation
Cut-slope
Lidar
Point clouds
Road asset inventory

ABSTRACT

An inappropriately maintained road cut-slope is likely to fail, resulting in landslides or falling rocks that compromise road safety. Thus, road managers need to know the location of dangerous slopes along the road in order to prevent these events from happening. In this article, we compare two different approaches for conducting the digitization of the road environment and the automatic detection and delimitation of road slopes: Mobile Laser Scanners (MLS) and Aerial Laser Scanners (ALS). The point clouds obtained using the first kind of devices are dense, rich in detail and generated from a ground perspective; the second type of scanners produce less dense clouds from a zenithal perspective. We explore what is the effect of the point cloud density and scanner point of view over the slope detection procedure. Two road segments from the Spanish A55 and A52 highways were used as study zones, and a total of 28.61 km were analyzed. Better detection and delimitation results were achieved when using the ALS data and its corresponding algorithm. It was observed that the higher point density and detail of the MLS clouds were not an advantage for the slope detection task, and that measuring the road from a terrestrial perspective affected in a negative way during the detection process: the crest of the slopes often remained unmeasured, hidden behind vegetation or man-made elements, thus resulting in the slopes not being complete in the MLS clouds. Meanwhile, the whole slope structure is scanned when the scene is measured from an aerial perspective, henceforth obtaining better detection rates despite the relatively low resolution. The findings of this study provide valuable information in the field of road asset management, and help road managers make decisions when choosing what technology to use for the data gathering process.

1. Introduction

A secure, reliable and sustainable road transportation system is of key importance to encourage profitable economic exchange and to ensure the safe movement of people [1,2]. However, keeping the infrastructure in an adequate operational condition can be a challenging task. Professionals in charge of its management are constantly required to come to difficult decisions regarding safety concerns, plan the construction of new road segments and design the maintenance schedule of the existing ones [3]. To correctly make critical choices, managers need to know, with fair accuracy, what the situation of the infrastructure is. Thus, roads and its most important assets must be measured through reliable sensors and standardized procedures and its working condition evaluated using trustworthy indicators [4].

The classic approach for the surveillance process relies on on-site inspections for data gathering and on posterior manual analysis of that obtained data. Performing the surveillance task in this fashion can result on incomplete or incorrect data sets, and scientific research has been produced to automate as many processes as possible and to account for these flaws. A more modern analysis paradigm relies on the usage of remote sensing devices for the digitization of the road environment and on the follow-up implementation of automatic data analysis procedures for feature extraction [5].

The digitization process of the road surface [6] and the traffic control elements [7] has been extensively studied. Using point clouds, methods for detecting pole like objects, road signals, road cracks, traffic lights, lane markings or trees have been successfully designed and put to practice [8]. Tunnel sections have also been successfully evaluated using point clouds, as in [9,10], and classification of entire scenes, using deep learning techniques, have also been conducted [11]. It is also

* Corresponding author.
E-mail addresses: anton.nunez.seoane@uvigo.gal (A. Núñez-Seoane), joaquin.martinez@uvigo.gal (J. Martínez-Sánchez), erik.rua@uvigo.gal (E. Rúa), parias@uvigo.gal (P. Arias).

https://doi.org/10.1016/j.measurement.2023.113919
Received 5 October 2023; Received in revised form 18 November 2023; Accepted 21 November 2023
Available online 23 November 2023

Table 1
Some investigations that have contributed to the field of slope surveillance.

Authors	Type of data used	Main contribution
[23] Riquelme et al.	TLS point cloud (PC)	A methodology for the geometric characterization of slopes in an automatic way
[11] Balado et al.	MLS PC	Detection of slopes (and other assets) using a Deep Learning approach
[22] Van Nieuwenhuizen et al.	Lidar DEM	Detection of embankments using a region growing algorithm
[26] Rúa et al.	ALS PC	Fast slope detection using cross-profile analysis
This article	ALS and MLS PCs	Comparison of MLS and ALS point cloud data sets for slope detection

possible to use RGB images for some detection tasks, as shown in [12] for signage and in [13] for crack damage, but these are often influenced by environmental conditions and are unreliable to some degree [14].

Apart from the pavement and the traffic elements, near-road slopes are another type of road asset that gain a lot of attention from researchers. Natural or human-made, slopes are a threat to road safety if they are not correctly maintained, since the failure of a slope results on falling blocks or landslides that can have great costs in terms of material and human life losses [15]. It is paramount for road managers to ensure the stability of the slopes using state of the art solutions. Numerous investigations have been conducted regarding slope stability [16], and the more common failure mechanisms are well known [17]. The more advanced research is nowadays directed towards the development of risk evaluation techniques based on statistical data [18,19] and on landslide/rockfall simulations and posterior design of effective protective measures [20,21].

Road slopes can be studied using Digital Elevation Models (DEMs) – using a similar approach to the one presented in [22] – but if the researchers need to evaluate the stability situation of the slope, point clouds are required. These data sets can offer information of great value regarding the geometrical definition – dip and dip direction – of the discontinuity sets of the slopes and of the slope itself. A highly regarded tool that automates the geometrical analysis process is the *Discontinuity Set Extractor Tool* (DSE Tool), which uses as input the point cloud data of slopes to find, through the implementation of an heuristic algorithm, these key features [23]. This tool was tested in clouds coming from Terrestrial Laser Scanners (TLS) [23,24] and in clouds obtained through the photogrammetric technique of *Structure from Motion* (SfM) [25].

The main drawback of the approach proposed in [23] is that it assumes a high quality point cloud as input, which makes necessary the displacement of the researcher to the location of the slope. This is a significant concern if we consider the job of managing a transportation network consisting on thousands of kilometers of roads. There is no time nor budget to examine every stretch of road looking for slopes. Mounting the laser scanner on a vehicle, such as an automobile – Mobile Laser Scanner (MLS) – or an airplane – Aerial Laser Scanner (ALS) –, and driving through or flying over an interest zone can help solve the problem. However, the large amount of data that can be obtained using ALS and MLS devices makes necessary the use of automatic search methods to find the slopes in the point clouds. To provide a tool to undertake this task, in [26] a methodology and its implementation were presented, using as data source low density ALS point clouds. In this article, we aim to expand that investigation by testing the there proposed workflow to the case of MLS data sets. The fundamental objective of this investigation is to compare the outcome obtained in [26] with detected slopes that result from the analysis of MLS point clouds, as we identified that no studies had been previously performed with the aim of determining the optimal way of digitizing the road environment (Table 1).

Thus, the main contribution of the present article is found in this result comparison. The conclusions driven from this analysis convey important information regarding the limitations shown by each type of cloud when used to analyze the road environment looking for dangerous slopes. The importance of the point of view of the scanner is observed in the results. Besides, we introduce a new, heavily modified, version of the detection algorithms presented in [26] to make them suitable to analyze MLS point clouds.

In Section 2, the applied methodology is explained. After that, the case of study used for testing the algorithms is presented in Section 3. Section 4 showcases the obtained results and Section 5 discusses them. A summary of the found conclusions is presented on Section 6 and possible future research lines are outlined in Section 7.

2. Methodology

In order to determine which data set is more useful for the automation of slope surveillance procedures, the same highway segments were studied using both ALS and MLS clouds. For each case, we ran a processing algorithm that automatically performed the detection and delimitation of slopes in the segment. Finally the quality of the results was measured using the parameters of precision, recall and F_{score}. The obtained values for each index were then compared to determine the more suitable scanning device for the slope detection task.

2.1. Main principles of the detection methodology

The core idea of the used analysis methodology is based on the study of the cross-profiles of the road, as they contain the key geometric properties of slope gradient and height. These values are used to perform a binary classification of the profiles, determining whether they belong or not to a slope. Finally, close slope-belonging profiles are clustered and the slopes delimited.

However, it is worth noting that each cloud type requires its own processing algorithm. In [26], an implementation of said core idea was designed to be applied to ALS data. In the present work, this is the approach used for processing aerial point clouds. This proposal, however, is not suitable for the analysis of MLS data, as it makes use of certain geometrical properties that are exclusive from the ALS clouds. Therefore, we designed a new method that could be employed for the analysis of MLS data sets. In the following subsections, both approaches are explained.

2.2. Analyzing ALS point clouds

This version of the methodology was extensively explained and discussed in [26]. For context, it can be summarized in four main steps:

- **Filtering of the original point cloud**: extraction of the ground points from the raw point cloud. A buffer around the road is calculated to reduce the number of points to be loaded.
- **Calculation of the points of each cross-profile**: cross-profiles are extracted by calculating the XY coordinates of the points of each profile and then retrieving the Z coordinate from the point cloud using a nearest neighbor interpolation.

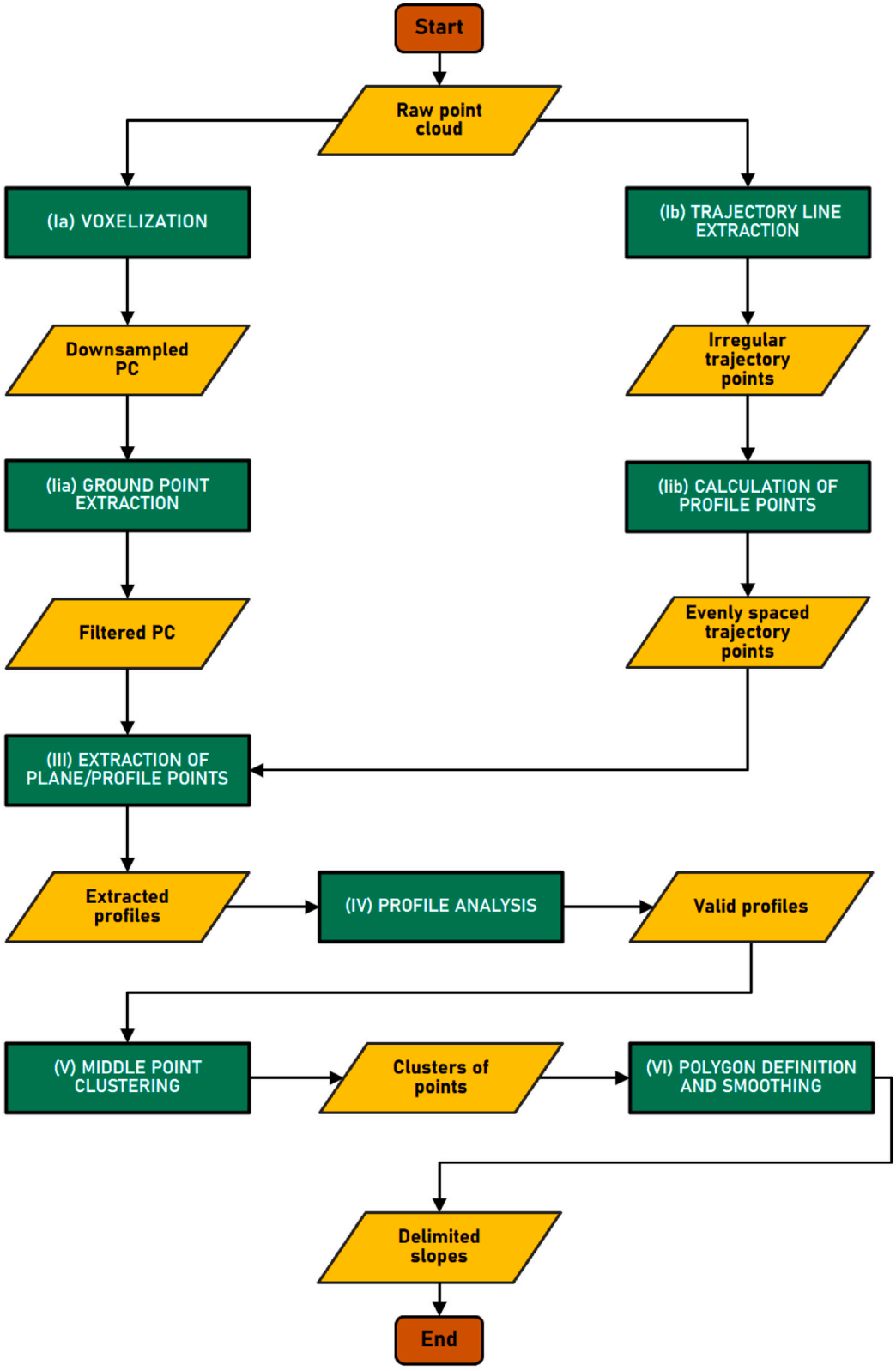

Fig. 1. Flow diagram of the processing method for the MLS point clouds. Green rectangles are for processes and yellow rhomboids are for data.

- **Analysis of each cross-profile**: a decision-tree-like algorithm is applied to the points on each cross-profile, considering a gradient threshold and a height threshold that must be defined by the user. The thresholds used on [26] were 40° and 6 m, respectively. Each profile that complies with these limits is considered as slope-belonging and the main toe and main crest points are calculated using the information provided by the values of the derivative of the profile. This derivative is numerically calculated.

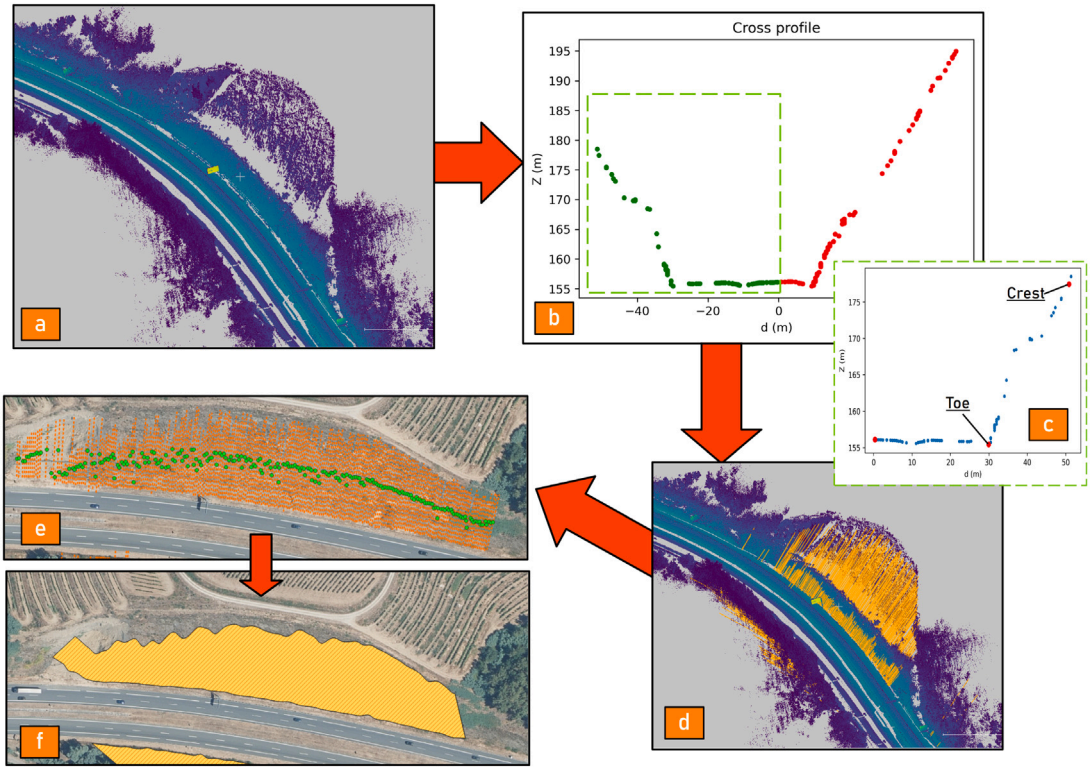

Fig. 2. General overview of the described process. *a* shows the raw point cloud. *b* is the representation of a cross profile, where each half is painted in a different color (red, green). In *c*, the toe and crest of one of the halves are depicted. Profiles belonging to a slope (orange lines) are drawn over the raw point cloud in *d*. In *e*, a set of clustered middle points is represented (green) over the displayed profiles (orange). The final slope is shown in *f*.

- **Slope delimitation**: consecutive valid profiles are considered to belong to the same slope and are thus grouped. Polygons that represent the area of the slopes are obtained using the toe and crest points from the profile groups as vertices. A shapefile containing these polygons is obtained, with information about mean gradient, mean height, mean dip direction and length.

2.3. Analyzing MLS point clouds

If the described ALS-oriented version of the algorithm is applied to MLS point clouds, slopes will not be correctly detected nor delimited, mainly because of the geometrical differences that the point of view of the scanner produces between the ALS and MLS point clouds. To maintain the cross-profile approach, some modifications had to be made to the ALS implementation, resulting on a new algorithmic solution prepared for the study of MLS data.

The MLS version is designed to use as input a georeferenced point cloud, stored as a *.las* file of version 1.6 or higher (Fig. 2, *a*), since the scan angle feature is used to extract the trajectory followed by the scanning vehicle (Fig. 1, Ib). The points with a very close to 0 scan angle are extracted and stored for later use. When this information has been obtained, the point cloud is downsampled via voxelization (Fig. 1, Ia), using a voxel size of 0.2 m. Then, the cloud is filtered in order to separate the ground from the non-ground points (Fig. 1, IIa), using the *visible point cloud utility* on the open3d library, which is an implementation of the method described in [27].

The extraction of the cross-profiles is then performed by first calculating a set of planes perpendicular to the trajectory followed by the scanning vehicle. This calculation is conducted using the trajectory points to estimate the normal vectors and to act as seeds for the planes. However, acquiring the trajectory using the scan angle approach results on a set of points not evenly distributed over the trajectory line, appearing scattered throughout. To ensure perpendicularity, a new set of evenly spaced points (Fig. 1, IIb) is calculated by repeatedly applying Eq. (1).

$$P_{next} = P_{initial} + d_p \cdot \hat{u}_r \tag{1}$$

Where P_{next} is the vector that represents the coordinates of the next point, $P_{initial}$ is the vector that represents the coordinates of the initial point, d_p is the distance between points – defined by the user – and $\hat{u}_r$ is the unit vector that defines the direction of advance of the trajectory points. The first $P_{initial}$ is the first point of the available scattered trajectory, while the calculated P_{next} becomes $P_{initial}$ on following iterations and $\hat{u}_r$ is the defining vector of the fitting regression line of the neighboring points of $P_{initial}$.

Then, the profile plane is defined by its normal vector, calculated as the difference between the seed point and the next point on the trajectory line. With the normal vector calculated, the distance to the plane of each point of the cloud is measured, using the dot product of the normal vector of the plane with each cloud-point to seed-point vector (Fig. 1, III). This is the same idea used in [10]. Only the points within a distance of 0.1 m are considered as contained on the plane. The profiles are thus extracted, as the points contained on the plane are the points of its corresponding cross-profile.

The key features of the profiles are then studied (Fig. 1, IV). As in the ALS method, height and gradient are the main geometric features that classify a certain profile as slope-belonging. Beginning with the separation of each profile in two halves (Fig. 2 *b*), a change in the frame of reference follows immediately after with the calculation of the centroid of the set of points. The relative distance to this point (d) is calculated for every other point on the plane, for then changing the reference frame from the classic three-dimensional XYZ Cartesian to a bidimensional dZ plane centered around the centroid. Then, for each semi-profile on the dZ plane, the toe detection analysis is performed, following the approach proposed in [28]. The toe position coincides with the point further away from the imaginary straight line (named

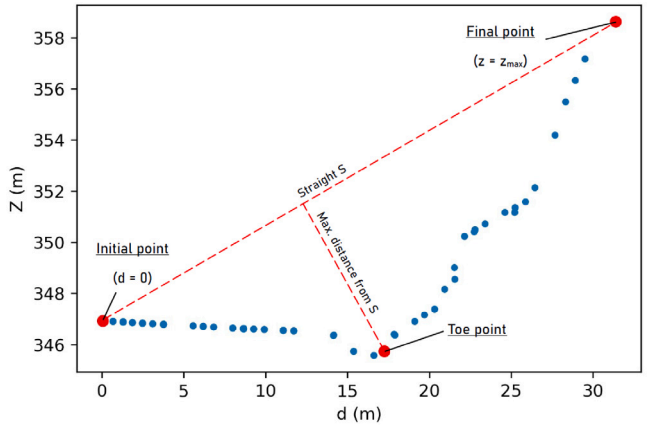

Fig. 3. Diagram summarizing the toe calculation process.

S, on Fig. 3) defined by the first point of the profile ($d = 0$) and its highest ($z = z_{max}$). The crest point is defined as the last point of the profile, as this is usually the best approach that can be obtained from the point of view of the MLS.

The final step of the process consists on the delimitation of the slopes. First, the central point of each profile is calculated, for then applying the DBSCAN algorithm [29] to perform a clusterization of those points (Fig. 1, V). As each central point corresponds to a toe-crest couple, when the central points are organized into clusters (Fig. 2 *e*), toes and crests are also effectively organized. This makes possible the delimitation of a polygon for each cluster of points (Fig. 1, VI). The spiky polygons that result from this delimitation are then processed by applying the Chaikin algorithm [30,31], a smoothing process that happens in an iterative way. For a given control polygon, defined by its vertices $\{P_0, P_1, \ldots, P_n\}$, a sequence of control points $\{Q_0, R_0, Q_1, R_1, \ldots, Q_{n-1}, P_{n-1}\}$, that represent the vertices of the smoothed polygon, is generated. These are calculated according to Eqs. (2) and (3).

$$R_i = 0.25P_i + 0.75P_{i+1} \tag{2}$$

$$Q_i = 0.75P_i + 0.25P_{i+1} \tag{3}$$

Where R_i and Q_i are the control points and P_i and P_{i+1} the vertices of the polygon to be smoothed.

This process can be applied repeatedly until the desired degree of smoothing is obtained. The number of iterations varies depending on the separation between cross profiles, with a higher number of iterations as the distance between profiles is reduced. In Fig. 2 *f*, the smoothed polygon is shown.

The final result of the proposed algorithm is a set of detected slopes in the study zone, represented by the necessary number of polygons, with information about height, dip (gradient), dip direction and length of each slope. Height, dip and dip direction are the average of heights, dips and dip directions of the profiles that compose the slope. Length is calculated measuring the length of the line formed by the toe points of the profiles.

2.4. Comparison of the obtained results

The final step of the methodology consists on the evaluation of the results obtained using both automation approaches. To compare the performance obtained with each data set, the quality of the detection and delimitation of the slopes is calculated, following the same ideas used in [26]. The results obtained after the automatic analysis of both ALS and MLS point clouds are compared with a slope data set manually acquired, gathered by expert engineers using a combination of remote sensing data – orthophotography and DTMs – and knowledge of the zone of study.

Both detection and delimitation performance were calculated and evaluated using the ratios of precision, recall and F_{score}. The general definition of these indices is as shown in Eqs. (4), (5) and (6) [32]:

$$P = \frac{TP}{TP + FP} \tag{4}$$

$$R = \frac{TP}{TP + FN} \tag{5}$$

$$F_{score} = 2 \cdot \frac{P \cdot R}{P + R} \tag{6}$$

Where P is the Precision value, R is the Recall value, TP represents the True Positives, FP the False Positives and FN the False Negatives.

When measuring detection performance, TP was considered to be the number of manual slopes detected correctly by the automatic algorithm, FN were manual slopes not detected using the point clouds, while FP were slopes detected using the automated approach that had no correspondence on real data. Thus, precision, recall and F_{score} of the detection phase are calculated using Eqs. (7)–(9).

$$P_{DT} = \frac{DT_{tp}}{DT_{tp} + DT_{fp}} \tag{7}$$

$$R_{DT} = \frac{DT_{tp}}{DT_{tp} + DT_{fn}} \tag{8}$$

$$F_{score(DT)} = 2 \cdot \frac{P_{DT} \cdot R_{DT}}{P_{DT} + R_{DT}} \tag{9}$$

Where P_{DT}, R_{DT} and $F_{score\ (DT)}$ are precision, recall and F_{score} for the detection case. DT_{tp} (detection true positives) are the number of manual slopes correctly detected, DT_{fp} (detection false positives) are the number of automatic slopes that do not correspond to a manual detection and DT_{fn} (detection false negatives) are the number of manual slopes not detected.

For the delimitation evaluation, the TP value represents the quantity of slope surface automatically measured that matches the manually delimited, the FN value is the area of the manual slopes not delimited, and the FP is the automatically delimited area that does not overlap with any manual area. Then, for the delimitation phase, precision, recall and F_{score} are calculated as shown by Eqs. (10), (11) and (12):

$$P_{DL} = \frac{DL_{tp}}{DL_{tp} + DL_{fp}} \tag{10}$$

$$R_{DL} = \frac{DL_{tp}}{DL_{tp} + DL_{fn}} \tag{11}$$

$$F_{score(DL)} = 2 \cdot \frac{P_{DL} \cdot R_{DL}}{P_{DL} + R_{DL}} \tag{12}$$

Where P_{DL}, R_{DL} and $F_{score\ (DL)}$ are precision, recall and F_{score} for the delimitation case. DT_{tp} (true positive delimitation) is the area of the delimited slopes correctly detected, DL_{fp} (false positive delimitation) is the automatically detected surface that should not have been delimited and DL_{fn} (false negative delimitation) is the area of the manual slopes that was not delimited.

3. Case of study

3.1. Selected road segments

Segments from the A55 and A52 highways, two roads of great strategic value, located in the South of Galicia, Spain, were selected as cases of study for the present work. The A55 connects the city of Vigo with the industrial zone of Porriño and with Portugal, while the A52 acts as a link between the South of Galicia and the rest of Spain. The selected locations had been previously studied in [26], where an inventory of the slopes was obtained by analyzing public ALS data.

Available MLS data allowed for the analysis of a total of 28.61 km from which 21.94 km corresponded to the A52 and 6.67 km to the A55 (Fig. 4).

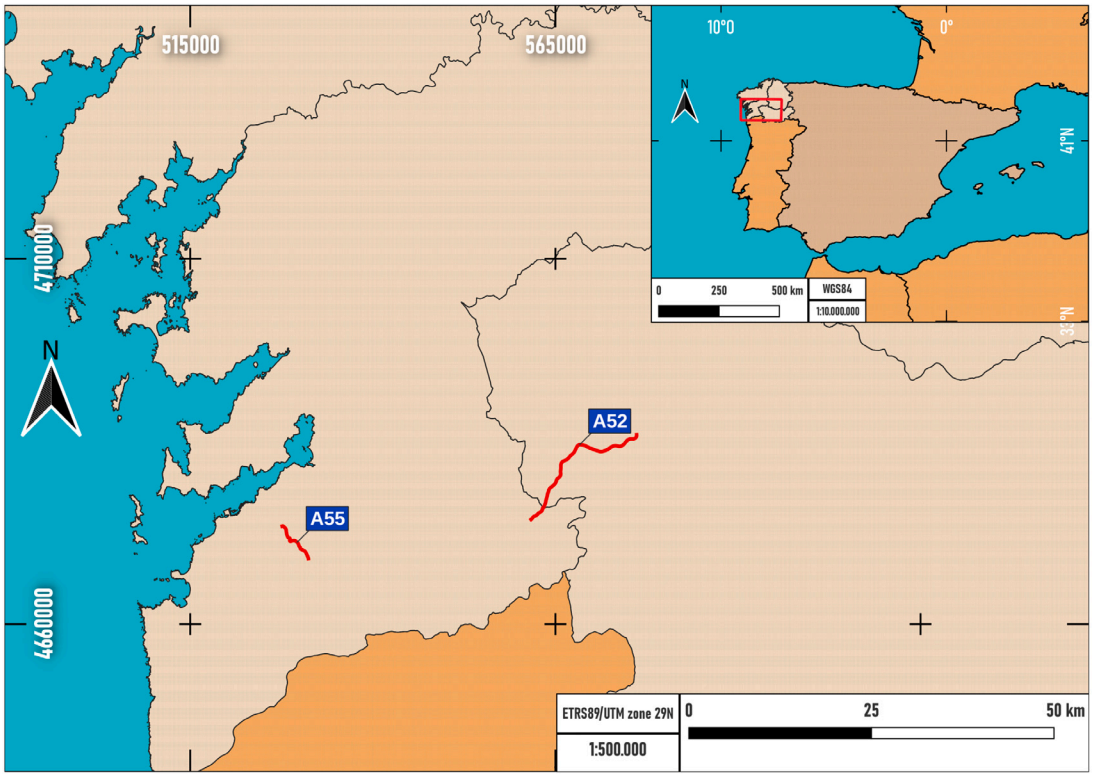

Fig. 4. Map showing the location of the studied segments from the A55 and A52.

3.2. Available data

Point clouds from the lidar branch of the Spanish PNOA (*Plan Nacional de Ortofotografía Aérea*) project were used as airborne laser scanner data. This project is managed and coordinated by the *Instituto Geográfico Nacional* [33], a publicly funded entity that is in charge of the geospatial information of Spain. Point clouds are available in the download center of the *Centro Nacional de Información Geográfica* (CNIG) [33]. Densities of these clouds range from 0.5 points/m^2 to 4 points/m^2 with some exceptions that reach 14 points/m^2. The Root Mean Square Error (RMSE) Z is of 0.2 m for any case. In our locations, the available clouds were of the lowest possible density of 0.5 points/m^2 and belonged to the most recent campaign, that took place between the years 2015 and 2016.

The Mobile Laser Scanner clouds were gathered using a custom mobile mapping system which integrates a lidar sensor (RIEGL VUX-1HA[22]) that is capable of 1.8 million measurements and 250 scan lines per second. To perform the mapping process of the infrastructure, the device was mounted on the roof of a vehicle which was then used to cover the road segments previously indicated. For georeferencing these clouds, a set of proprietary software was used, coupled with the open Real Time Positioning System of the IGN.

4. Results

The selected locations were analyzed applying the described processes in Section 2. The objective of the algorithms were slopes with at least 6 m of height and 40° of gradient. Regarding the cross-profile distance, the ALS clouds were analyzed in [26] using a separation of 10 m, as this separation was deemed optimal in that study. The MLS point clouds were analyzed using this distance between profiles, and also 20 m and 1 m to check how this parameter affected performance. Table 2 shows the results obtained for each case.

Computing time was measured as well, presented as absolute processing time (Fig. 5) and as specific processing time per analyzed kilometer (Fig. 6).

Table 2
Detection rates for both cases of study. "Det." is for the number of detected slopes, while "% of man." is for the percentage of manually detected slopes automatically detected.

Iteration	A55		A52	
	Det.	% of man.	Det.	% of man.
Manual	9	–	46	–
ALS-10	9	100	44	95.65
MLS-20	3	33.33	27	58.70
MLS-10	6	66.67	32	69.57
MLS-1	8	88.89	40	86.96

Table 3
For each case of study and profile separation, delimitation true positives (DT_{tp}), false negatives (DT_{fn}) and false positives (DT_{fn}) detected slopes.

Iter.	A55			A52		
	DT_{tp}	DT_{fn}	DT_{fp}	DT_{tp}	DT_{fn}	DT_{fp}
ALS-10	9	0	0	43	3	0
MLS-20	3	6	0	27	19	0
MLS-10	6	3	0	32	14	0
MLS-1	8	1	2	40	6	1

The algorithms were written using Python 3.9 as the main programming language, and were run on a machine that mounted an AMD Ryzen 9 6900 HX as CPU and an NVIDIA GeForce GTX 3070 Ti Laptop as GPU.

4.1. Detection performance

In Table 3, raw results obtained after the detection procedure are presented, while Table 4 showcases the obtained values for precision in detection (P_{DT}), recall in detection (R_{DT}) and F_{score} in detection ($F_{score\ (DT)}$), after using the Eqs. (7), (8) and (9) over the data of Table 3. The value of P_{DT} measures how many slopes of the total

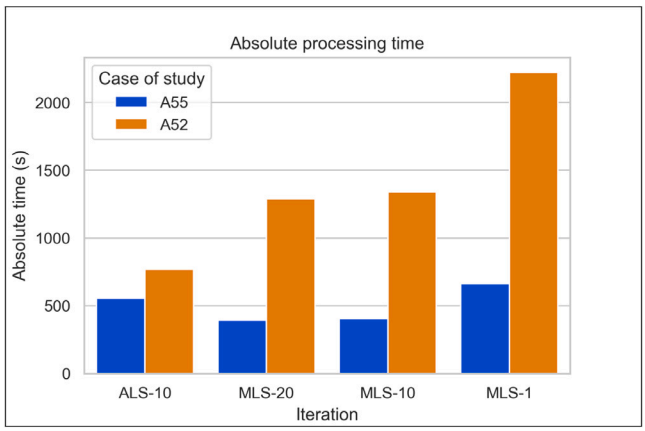

Fig. 5. Processing time required for each study, in seconds.

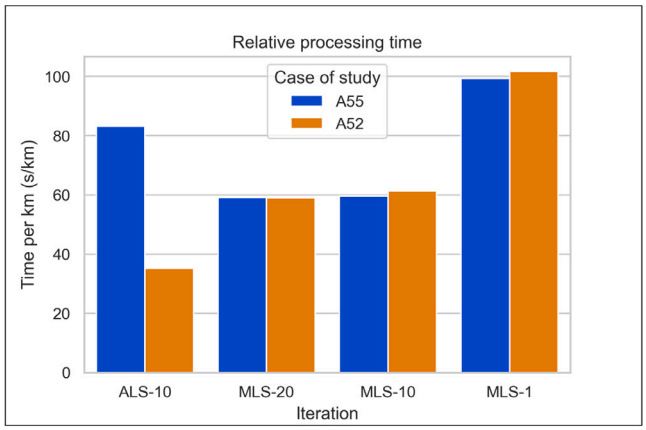

Fig. 6. Relative processing time required for each case of study, in seconds per kilometer.

Table 4
Metrics of detection performance for each case of study and profile separation. P_{DT} stands for precision in detection while R_{DT} stands for recall in detection. $F_{score\ (DT)}$ is the F_{score} in detection.

Iter.	A55			A52		
	P_{DT} (%)	R_{DT} (%)	$F_{score\ (DT)}$	P_{DT} (%)	R_{DT} (%)	$F_{score\ (DT)}$
ALS-10	100	100	1.0000	100	93.48	0.9663
MLS-20	100	33.33	0.5000	100	58.70	0.7398
MLS-10	100	66.67	0.8000	100	69.57	0.8205
MLS-1	80	88.89	0.8421	97.56	86.97	0.9196

detected were slopes in reality, the value of R_{DT} measures how many of the real slopes were retrieved, and $F_{score\ (DT)}$ can be interpreted as the percentage of correctly detected slopes found in the total of automatic and manual slopes.

High precision is obtained in both cases of study, reaching 100% for every case except for the MLS-1 iteration, where lower values of 80% and 97.56% P_{DT} are obtained for the A55 and A52, respectively. In the ALS case, 100% precision is achieved in both highways.

Regarding recall values, more slopes are detected as the separation between profiles is diminished. When the largest separation −20 m- is used, only a third of the slopes is detected in the A55 (R_{DT} = 33.33%) and around a 60% in the A52 (R_{DT} = 58.70%), but improvement is observed as the distance between profiles is reduced. The best results derived from the MLS clouds are obtained with a separation between profiles of 1 m, detecting 8 out of 9 slopes in the A55 (R_{DT} = 88.89%) and 40 out of 46 in the A52 (R_{DT} = 86.97%). This comes at the expense of false positives, 2 for the A55 and 1 for the A52. When ALS and MLS results are compared, the aerial scanner wins in both highways, as it detects 9 out of 9 slopes in the A55 (R_{DT} = 100%) and 43 out of 46 in the A52 (R_{DT} = 93.48%).

Considering that the values of P_{DT} are similar on every case, the values of $F_{score\ (DT)}$ mainly depend on R_{DT}. Therefore, the same trends outlined for recall are true for $F_{score\ (DT)}$: the best overall value is obtained for the case of ALS clouds (0.9663), while the best MLS performance is achieved for the 1 m separation case (0.9196).

Table 5
For each case of study and profile separation, true positive delimited area (DL_{tp}), false negative delimited area (DL_{fn}) and false positive delimited area (DL_{fp}).

Iter.	A55			A52		
	DL_{tp} (m^2)	DL_{fn} (m^2)	DL_{fp} (m^2)	DL_{tp} (m^2)	DL_{fn} (m^2)	DL_{fp} (m^2)
ALS-10	8,241	5,559	4522	145,915	51,138	32,825
MLS-20	3,944	9,857	1,814	82,044	115,009	12,395
MLS-10	7,008	6,793	3,067	87,671	109,382	12,877
MLS-1	9,729	4,072	7,919	127,341	69,712	25,774

Table 6
For each case of study and profile separation, precision (P_{DL}), recall (R_{DL}) and F_{score} of the delimitation process ($F_{score\ (DL)}$).

Iter.	A55			A52		
	P_{DL} (%)	R_{DL} (%)	$F_{score\ (DL)}$	P_{DL} (%)	R_{DL} (%)	$F_{score\ (DL)}$
ALS-10	64.57	59.72	0.6205	81.64	74.05	0.7766
MLS-20	68.50	28.58	0.4033	86.88	41.64	0.5629
MLS-10	69.56	50.78	0.5870	87.19	44.49	0.5892
MLS-1	55.13	70.50	0.6187	83.17	64.62	0.7273

4.2. Delimitation performance

Performance evaluation of the delimitation task is conducted by comparing the area of the automatically delimited slopes with that of the manual slopes. The percentage of the automatic area that coincides with the manual is the precision in delimitation (P_{DL}) and the percentage of the manual area that is recovered is represented by the recall in delimitation value (R_{DL}). The $F_{score\ (DL)}$ metric shows the percentage of the combination of automatic and manual areas that is shared among both data sets. Table 5 shows the values obtained after the area calculation process, conducted in the same manner as in [26], using the GIS software QGIS. These values are then processed using Eqs. (10)–(12) to calculate P_{DL}, R_{DL} and $F_{score\ (DL)}$, respectively. Table 6 shows the obtained values for these indices.

For the delimitation using the MLS clouds, the precision obtained in the A55 highway is between 68.50% and 69.56% for the cases where no false positive slopes are detected (MLS-20 and MLS-10). However, when false positives appear, this metric drops to 55%. In terms of recall, it increases when the distance between profile decreases, going from the 28.58% of the 20 m separation to a 70.50% with the 1 m separation. $F_{score\ (DL)}$ also improves with the reduction of distance, reaching a maximum of 0.6187 for the MLS-1 case. The behavior exhibited in the A52 is no different, with a similar precision value for the MLS-20 and MLS-10 cases (86.88 and 87.19%, respectively) and a drop for the MLS-1 (83.17%) because of the detected false positive. For the recall, the more the distance between profiles is reduced, the better the results, going from a 41.64% to a 64.62%. The maximum F_{score} is obtained when the separation between profiles is 1 m, with a value of 0.7273.

The performance obtained using the MLS clouds comes very close to that of the ALS method, but ultimately does not get as good results. If the best cases are compared, in the A55 the MLS-1 F_{score} of 0.6187 is slightly inferior to the 0.6205 of the ALS clouds, while in the A52 the difference is greater, with a 0.7273 for the MLS and a 0.7766 for the ALS.

5. Discussion

In [26], near-road slopes were automatically detected and delimited using open access lidar point cloud data. In the present article, we wanted to expand the ideas presented there and test if MLS point clouds could be used for the same task. Therefore, we adapted the algorithm proposed on that article to process mobile lidar point clouds, more dense and rich in detail. A direct comparison of the obtained results shows how the detection performance on the ALS clouds is noticeably better than that obtained with the MLS data, and that the delimitation performance also does not increase in any way, as the $F_{score\ (DT)}$ metric is very similar in both cases of study for the two types of data. The increase in point density diminished the detection rate of the slopes, going down from 9 out of 9 – ALS – to 8 out of 9 – MLS – in the A55 and from 44 out of 46 – ALS – to 40 out of 46 – MLS – in the A52 (visit again Table 2). This reduction in performance can be mainly explained by the different points of view from which the point clouds were measured – aerial versus terrestrial – and by the assumptions made during the design and implementation of an heuristic algorithm like the one proposed.

We found of significance the comparison that can be made between our work and [22], where the authors detect embankments using lidar DEM's as a data source — while embankments are not slopes, their shape is fairly similar. Among 8 cases of study presented in that work, the best overall performance was of a 94.0% precision and an 81.8 % recall for the detection task. For our MLS clouds, the best performance is obtained for the case of the MLS-1 iteration: P_{DT} of 97.56% and an R_{DT} of 86.97% in the A52, and a P_{DT} = 80% and an R_{DT} = 88.89% for the A55. As it is clearly seen, the results obtained in the A52 beat those of [22], while the numbers of the A55 case remain behind. In any case, both the MLS iteration and [22] perform worse than when the ALS data is used.

Differences between the ALS and MLS point clouds can be observed in terms of point cloud density and point of view (POV). The used ALS point clouds are a low density measurement of ground surface obtained using a scanner mounted on an airplane, this is, the terrain is observed from a zenithal perspective. The MLS clouds are, on the other hand, high density measurements obtained as the vehicle mounting the scanner traverses the study zone. The difference in POV is of significance in this study, as it is observed that the crest of the slope is not correctly measured by the MLS, while the ALS is able to obtain a more complete depiction of the whole structure, despite having less points representing that reality. The crest zone usually remains partially defined on the MLS clouds, as it is occluded by obstacles located on lower levels of the face of the slope, such as trees or man-made structures. The used methodology and its successful implementation assume that a slope is defined, on each cross-profile, by two points: the crest and the toe. If one of those is not correctly defined on the profile, the algorithm will fail to recognize it as slope-belonging. This is the main reason why when comparing ALS and MLS results obtained using the same cross-profile separation (10 m), less slopes are detected on the MLS clouds. As the crest is partially occluded in the MLS clouds, a higher number of points must be sampled to find profiles where the crest point is actually defined. This statement is confirmed by the fact that detection and delimitation quality increase when the distance between cross profiles is reduced (see Tables 4 and 6). The high point cloud density is not important for the proposed methodology, and only contributes to the increase in processing time, as it can be seen in Figs. 5 and 6.

It is clear, then, that detection rates and delimitation performance not only do not improve when using high density MLS point clouds, but also get worse as the point cloud POV causes the crest point to remain unmeasured in many occasions, thus reducing detection opportunities. Point cloud density is not quite as important for the detection and delimitation with the proposed algorithm, as it only really requires two points on the profile to perform this task. This suggests that the optimal way of dealing with the detection and delimitation is to use ALS point clouds, as the processing time is relatively short while offering better results than those obtained using MLS data.

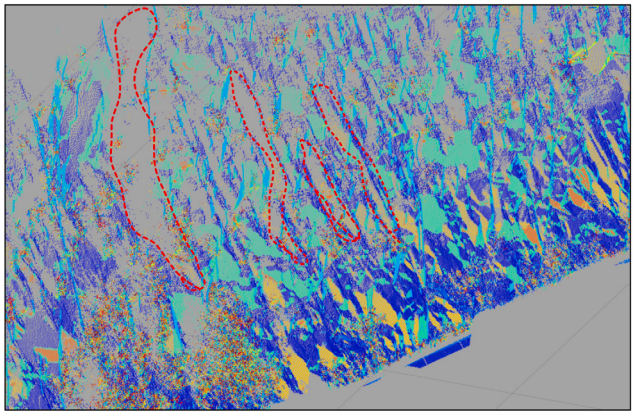

Fig. 7. Slope point cloud processed with the Discontinuity Set Extractor Tool. Different colors represent different discontinuity families. Red discontinuous lines show some of the places in the cloud where no points were measured, and thus no discontinuity family was detected.

However, it is worth noting that the findings obtained in this study cannot be extrapolated to other types of roads. While we have concluded that ALS point clouds are better data sets for automating the detection and delimitation of slopes in highways, we can only apply this statement to that kind of environments, as no other types were studied in the present investigation. The conclusions should not be extrapolated to secondary or urban roads, since no experiments were conducted to verify if ALS still offers better detection results for roads of smaller capacity.

As a final observation, we would like to point out that the type of clouds used in this study cannot be integrated in the workflow for stability evaluation of slopes. Several works [23–25] have showcased how useful point clouds can be for the geometrical characterization of slopes, even partially automating the process. The point clouds used on those investigations were highly detailed data sets obtained using several scanning positions, resulting on a point cloud with no occlusions or shadowy areas. As for the clouds used in this study, none of them are usable to perform automatic discontinuity set extraction over them. The ALS clouds do not offer enough points to even try the tool over them, while the MLS clouds, which do have enough points available, cannot be used because of limitations derived from the point of view of the scanner. Upper zones of the slopes remain unmeasured, with no points defining them (as an example, see Fig. 7), hence resulting on an incomplete geometrical definition of the families of the slope, precluding, as a consequence, its stability evaluation.

6. Conclusions

The purpose of this investigation was to evaluate how Mobile Laser Scanner point clouds could facilitate the surveillance operation of near-road safety-critical slopes. This evaluation was performed using MLS and ALS clouds to study the same segment of a spanish highway, for then directly comparing the obtained results. More slopes were detected and were more accurately delimited when using the ALS data sets than when point clouds came from MLS scans. This can be explained because in the MLS data sets the slopes are not correctly captured by the laser scanner; occlusions generated because of the from-ground point of view of the MLS scanner often reduced the overall quality of the MLS cloud.

These facts drive to the conclusion that open data ALS point clouds are, right now, preferable data sources for the detection and delimitation of near-road slopes, as MLS data sets, while highly detailed,

provide no advantage to the detection of massive structures. However, this data sets remain useful for other tasks, such as signage inventory or crack detection. Minding the results presented in this article, we recommend using ALS point cloud data for easily building a slope inventory data set, and to use it to design an efficient characterization campaign of the slopes that would need to involve a more detailed *in situ* analysis of its structure.

7. Future work

Lastly, we would like to signal towards two interesting lines of research that would continue the showcased investigation. For the first, it is worth noting that no deep learning techniques were applied to process any of the available data sets. However, these techniques have provided remarkably good results in different areas of knowledge, and their convenience and performance when introduced into the field of slope monitoring tasks should be evaluated. Neural networks could be specially useful when deployed as a tool for improving the delimitation of the slopes, the weakest point of the deterministic approaches evaluated in this article. The other area where new research should be focused on is the study of how other sensors, different from lidar, can contribute in the stability assessment process. Data about the type of rock or the amount of water flow, among other parameters, is needed to evaluate the stability of a slope, and such kind of data is not obtainable using laser scanners. Investigation should be conducted in order to find out if other types of sensors, such as RGB, or time-of-flight cameras, can measure relevant properties of the slopes, this way advancing towards a more automated and accurate slope stability assessment process.

CRediT authorship contribution statement

Antón Núñez-Seoane: Conceptualization, Formal analysis, Investigation, Methodology, Software, Validation, Writing – original draft, Writing – review & editing. **Joaquín Martínez-Sánchez:** Conceptualization, Project administration, Supervision, Writing – review & editing. **Erik Rúa:** Data curation, Formal analysis, Methodology. **Pedro Arias:** Conceptualization, Project administration, Supervision, Writing – review & editing.

Declaration of competing interest

The authors declare that they have no known competing financial interests or personal relationships that could have appeared to influence the work reported in this paper.

Data availability

The data that has been used is confidential.

Acknowledgments

This publication is part of the project "RoadS2Win" with reference PID2022-140662OB-I00 funded by the Government of Spain through MCIN/AEI/10.13039/501100011033 as part of the "ERDF A Way of Making Europe". This work has also received funding from the European Union's Horizon 2020 research and innovation program under grant agreement No. 955337. It reflects only the authors' views. Neither the European Climate, Infrastructure, and Environment Executive Agency (CINEA) nor the European Commission is in any way responsible for any use that may be made of the information it contains. Funding for open access charge: Universidade de Vigo/CISUG.

References

[1] United Nations, Sustainable development goal 9, 2023, https://www.un.org/sustainabledevelopment/infrastructure-industrialization/.
[2] E. Ivanová, J. Masárová, Importance of the road infrastructure in the economic development and competitiveness, Econ. Manag. 18 (2) (2013) 263–274, http://dx.doi.org/10.5755/j01.em.18.2.4253, http://www.ecoman.ktu.lt/index.php/Ekv/article/view/4253.
[3] L. Persia, D.S. Usami, F. De Simone, V.F.D.L. Beaumelle, G. Yannis, A. Laiou, S. Han, K. Machata, L. Pennisi, P. Marchesini, M. Salathè, Management of road infrastructure safety, Transp. Res. Procedia 14 (2016) 3436–3445, http://dx.doi.org/10.1016/j.trpro.2016.05.303, https://linkinghub.elsevier.com/retrieve/pii/S235214651630309X.
[4] A. Amekudzi, S. McNeil, Infrastructure Reporting and Asset Management: Best Practices and Opportunities, American Society of Civil Engineers, Reston, VA, 2008, http://dx.doi.org/10.1061/9780784409589, https://ascelibrary.org/doi/book/10.1061/9780784409589.
[5] M. Elhashash, H. Albanwan, R. Qin, A review of mobile mapping systems: From sensors to applications, Sensors 22 (11) (2022) 4262, http://dx.doi.org/10.3390/s22114262, https://www.mdpi.com/1424-8220/22/11/4262.
[6] W. Cao, Q. Liu, Z. He, Review of pavement defect detection methods, IEEE Access 8 (2020) 14531–14544, http://dx.doi.org/10.1109/ACCESS.2020.2966881, https://ieeexplore.ieee.org/document/8960347/.
[7] M. Li, X. Li, D. Wu, L. Zou, X. Huang, Digitizing and inventorying traffic control infrastructures: A review of practices, Transp. Res. Interdiscip. Perspect. 21 (2023) 100879, http://dx.doi.org/10.1016/j.trip.2023.100879, https://linkinghub.elsevier.com/retrieve/pii/S2590198223001264.
[8] Soilán, Sánchez-Rodríguez, Río-Barral, Perez-Collazo, Arias, Riveiro, Review of laser scanning technologies and their applications for road and railway infrastructure monitoring, Infrastructures 4 (4) (2019) 58, http://dx.doi.org/10.3390/infrastructures4040058, https://www.mdpi.com/2412-3811/4/4/58.
[9] A. Wróblewski, J. Wodecki, P. Trybała, R. Zimroz, A method for large underground structures geometry evaluation based on multivariate parameterization and multidimensional analysis of point cloud data, Energies 15 (17) (2022) 6302, http://dx.doi.org/10.3390/en15176302, https://www.mdpi.com/1996-1073/15/17/6302.
[10] C. Yi, D. Lu, Q. Xie, J. Xu, J. Wang, Tunnel deformation inspection via global spatial axis extraction from 3D raw point cloud, Sensors 20 (23) (2020) 6815, http://dx.doi.org/10.3390/s20236815, https://www.mdpi.com/1424-8220/20/23/6815.
[11] Balado, Martínez-Sánchez, Arias, Novo, Road environment semantic segmentation with deep learning from MLS point cloud data, Sensors 19 (16) (2019) 3466, http://dx.doi.org/10.3390/s19163466, https://www.mdpi.com/1424-8220/19/16/3466.
[12] S.B. Wali, M.A. Abdullah, M.A. Hannan, A. Hussain, S.A. Samad, P.J. Ker, M.B. Mansor, Vision-based traffic sign detection and recognition systems: Current trends and challenges, Sensors 19 (9) (2019) 2093, http://dx.doi.org/10.3390/s19092093, https://www.mdpi.com/1424-8220/19/9/2093.
[13] H.S. Munawar, A.W.A. Hammad, A. Haddad, C.A.P. Soares, S.T. Waller, Image-based crack detection methods: A review, Infrastructures 6 (8) (2021) 115, http://dx.doi.org/10.3390/infrastructures6080115, https://www.mdpi.com/2412-3811/6/8/115.
[14] M. Tsogas, N. Floudas, P. Lytrivis, A. Amditis, A. Polychronopoulos, Combined lane and road attributes extraction by fusing data from digital map, laser scanner and camera, Inf. Fusion 12 (1) (2011) 28–36, http://dx.doi.org/10.1016/j.inffus.2010.01.005, https://linkinghub.elsevier.com/retrieve/pii/S1566253510000199.
[15] M. Papathoma-Köhle, M. Kappes, M. Keiler, T. Glade, Physical vulnerability assessment for alpine hazards: state of the art and future needs, Nat. Hazards 58 (2) (2011) 645–680, http://dx.doi.org/10.1007/s11069-010-9632-4, http://link.springer.com/10.1007/s11069-010-9632-4.
[16] S. Kumar, S.S. Choudhary, A. Burman, Recent advances in 3D slope stability analysis: a detailed review, Model. Earth Syst. Environ. 9 (2) (2023) 1445–1462, http://dx.doi.org/10.1007/s40808-022-01597-y, https://link.springer.com/10.1007/s40808-022-01597-y.
[17] P. Ramírez Oyanguren, L.R. Alejano Monge, Mecánica de rocas : fundamentos e ingeniería de taludes, No. 727, Red DESIR, Madrid, 2004, https://oa.upm.es/14183/.
[18] S.A.H. Gardezi, N.A. Usmani, X.-q. Chen, N. Ikram, S. Ahmad, S. Wani, Application of techniques for landslide susceptibility prediction along an earthquake-affected road section in Kashmir Himalaya, Geol. J. 58 (2) (2023) 849–882, http://dx.doi.org/10.1002/gj.4630, https://onlinelibrary.wiley.com/doi/10.1002/gj.4630.
[19] D. Tiranti, L. Mallen, G. Nicolò, Rockfall hazard estimation and related applications for a preliminary risk assessment at regional scale: an example from northwestern Italian Alps, Landslides 20 (8) (2023) 1691–1704, http://dx.doi.org/10.1007/s10346-023-02060-4, https://link.springer.com/10.1007/s10346-023-02060-4.

[20] H. Al-Budairi, Z. Gao, A. Steel, Numerical modelling of double-twisted wire mesh for low-energy rockfall catch fences, Geosciences 13 (6) (2023) 180, http://dx.doi.org/10.3390/geosciences13060180, https://www.mdpi.com/2076-3263/13/6/180.

[21] Z.-f. Wang, H.-d. Liu, S.-m. He, D. Bi, Field investigation and numerical simulation on rockfalls in Zhangmu town, Tibet, China, J. Mt. Sci. 19 (3) (2022) 740–755, http://dx.doi.org/10.1007/s11629-021-7095-6, https://link.springer.com/10.1007/s11629-021-7095-6.

[22] N. Van Nieuwenhuizen, J.B. Lindsay, B. DeVries, Automated mapping of transportation embankments in fine-resolution LiDAR DEMs, Remote Sens. 13 (7) (2021) 1308, http://dx.doi.org/10.3390/rs13071308, https://www.mdpi.com/2072-4292/13/7/1308.

[23] A.J. Riquelme, A. Abellán, R. Tomás, M. Jaboyedoff, A new approach for semi-automatic rock mass joints recognition from 3D point clouds, Comput. Geosci. 68 (2014) 38–52, http://dx.doi.org/10.1016/j.cageo.2014.03.014, https://linkinghub.elsevier.com/retrieve/pii/S0098300414000740.

[24] A.J. Riquelme, R. Tomás, A. Abellán, Characterization of rock slopes through slope mass rating using 3D point clouds, Int. J. Rock Mech. Min. Sci. 84 (2016) 165–176, http://dx.doi.org/10.1016/j.ijrmms.2015.12.008, https://linkinghub.elsevier.com/retrieve/pii/S1365160915300939.

[25] R. Tomás, A. Riquelme, M. Cano, J.L. Pastor, J.I. Pagán, J.L. Asensio, M. Ruffo, Evaluación de la estabilidad de taludes rocosos a partir de nubes de puntos 3D obtenidas con un vehículo aéreo no tripulado, Rev. Teledetección (55) (2020) 1–15, http://dx.doi.org/10.4995/raet.2020.13168, https://polipapers.upv.es/index.php/raet/article/view/13168.

[26] E. Rúa, A. Núñez-Seoane, P. Arias, J. Martínez-Sánchez, Automatic detection to inventory road slopes using open LiDAR point clouds, Int. J. Appl. Earth Obs. Geoinf. 118 (2023) 103225, http://dx.doi.org/10.1016/j.jag.2023.103225, https://linkinghub.elsevier.com/retrieve/pii/S156984322300047X.

[27] S. Katz, A. Tal, R. Basri, Direct visibility of point sets, ACM Trans. Graph. 26 (3) (2007) 24, http://dx.doi.org/10.1145/1276377.1276407, https://dl.acm.org/doi/10.1145/1276377.1276407.

[28] H. Mitásová, E. Hardin, M.J. Starek, R.S. Harmon, M. Overton, Landscape dynamics from LiDAR data time series, 2011, https://api.semanticscholar.org/CorpusID:16773542.

[29] M. Ester, H.-P. Kriegel, X. Xu, A density-based algorithm for discovering clusters in large spatial databases with noise, in: Proceedings of the Second International Conference on Knowledge Discovery and Data Mining, KDD-96, 1996, pp. 226–231.

[30] G.M. Chaikin, An algorithm for high-speed curve generation, Comput. Graph. Image Process. 3 (4) (1974) 346–349, http://dx.doi.org/10.1016/0146-664X(74)90028-8, https://www.sciencedirect.com/science/article/pii/0146664X74900288.

[31] R. Riesenfeld, On Chaikin's algorithm, Comput. Graph. Image Process. 4 (3) (1975) 304–310, http://dx.doi.org/10.1016/0146-664X(75)90017-9, https://linkinghub.elsevier.com/retrieve/pii/0146664X75900179.

[32] D.M.W. Powers, Evaluation: from precision, recall and F-measure to ROC, informedness, markedness and correlation, 2020, CoRR arXiv:2010.16061.

[33] Centro de Descargas del Centro Nacional de Información Geográfica (CNIG), 2023, https://centrodedescargas.cnig.es/CentroDescargas/index.jsp.